

# Prediction of an undimerized, insulating, antiferromagnetic ground-state in halogen-bridged linear-chain Ni compounds

V. I. Anisimov, R. C. Albers, and J. M. Wills

*Los Alamos National Laboratory, Los Alamos, New Mexico 87545*

M. Alouani and J. W. Wilkins

*Department of Physics, The Ohio State University, Columbus OH 43210-1368*

(October 1994)

## Abstract

A parameter-free, mean-field, multi-orbital Hubbard model with nonspherical Coulomb and exchange interactions, implemented around all-electron local-density approximation (LDA) calculations, correctly predicts the band-gap energy, the absence of dimerization, and the antiferromagnetic ground state of halogen-bridged linear-chain Ni compounds. This approach also reproduces the insulating ground state and dimerization in PtX linear-chain compounds in agreement with experiment and previous calculations.

71.20.Hk, 71.25.Tn, 71.45.Nt, 71.38.+i, 71.45.Nt

arXiv:cond-mat/9507104v1 24 Jul 1995

The halogen-bridged transition-metal linear-chain compounds, referred to as MX compounds because of their alternating transition-metal atoms M and halogen atoms X, form weakly coupled linear-chain-like structures, and are of considerable interest [1–15] due to a rich and accessible phase diagram [2–12]. More specifically, experimentalists can now tune the strength of the charge-density wave (CDW) and spin-density wave (SDW) [4,7] and induce phase transitions from an CDW to an SDW state [3]. First-principles density-functional calculations of neutral PtX compounds have shown clearly that (1) the mechanism of the dimerization and the insulating ground state in the MX chain systems is due to an electron-phonon coupling along the chain, and (2) the ligand structure is essential for the correct description of ground-state properties [8]. New high-quality data on single crystals are challenging our understanding of the electronic structure of these low-dimensional systems [2–7]. The Ni MX compounds, which are normally in an SDW state, change to a mixed SDW/CDW state by a simple substitution of the counterion  $\text{Cl}^-$  with perchlorite  $\text{ClO}_4^-$  [7]. In a recent Peierls-Hubbard model study, local defect excitations in NiBr are found also to exhibit lattice distortion relative to the undistorted ground state [10]. It is interesting to mention that in the Ni compounds the electronic structure at the vicinity of Fermi level is the one dimensional equivalent of the undoped cuprate superconductor materials, where the local spin-polarized density approximation (LSDA) calculations predicted a non-magnetic metallic state instead of the observed antiferromagnetic insulating state. Here again the LSDA failed to reproduce the ground state properties of the Ni compounds.

In this Letter we study the electronic properties of both CDW and SDW chains by means of a newly developed mean-field, multi-orbital Hubbard model, called “LDA + U”, that has nonspherical Coulomb and exchange interactions and is implemented around all-electron local-density approximation (LDA) calculations with a linear muffin-tin orbital basis-set [16]. This model enables us to extend our previously successful LDA study of CDW MX systems [8,9] to also, for the first time, explain from first-principles the magnetic SDW systems. It predicts that the ground state for the NiX (X= Cl or Br) compounds is undimerized, insulating, and a low-spin antiferromagnetic, in good agreement with experiment [7]. The

large octahedral ligand-field splitting  $\Delta_0 = e_g - t_{2g} \approx 4$  eV produces a low-spin electronic configuration  $(t_{2g})^6(e_g)^1$  of the  $\text{Ni}^{+3}$ . It also predicts that the ground state of the PtX (X=Cl or I) linear-chain compounds is insulating and dimerized in agreement with our earlier calculations [8]. We have to stress that our calculations are based on a parameter-free model that uses a constrained LDA determination for the Coulomb and exchange interactions.

All the results presented in this Letter have been obtained using the ‘‘LDA + U’’ method, which is extensively described elsewhere [16]. Here we stress that the main feature of the model is to introduce a discontinuity in the LDA one-electron potential for integer change in orbital occupancy. The nonsphericity of the Coulomb and exchange interactions, i.e., the  $d$ -orbital occupation dependence on the orbital angular-momentum quantum number  $m$  and  $m'$ , is important for a good description of the magnetic moment of the MX chains.

The  $d_{3z^2-r^2}$  orbital, whose polarization dominates the magnetic moment, is also important in controlling the bonding, the dimerization, and the magnetism in these systems. The total energy and potentials include the exchange and the nonsphericity of the Coulomb  $d$ - $d$  interaction:

$$E = E_{LDA} - [UN(N-1)/2 - JN(N-2)/4] + \frac{1}{2} \sum_{m,m',\sigma} U_{mm'} n_{m\sigma} n_{m'-\sigma} + \frac{1}{2} \sum_{m \neq m', m', \sigma} (U_{mm'} - J_{mm'}) n_{m\sigma} n_{m'\sigma} \quad (1)$$

The screened Coulomb  $U$  and exchange  $J$  parameters are calculated self-consistently in the supercell approximation as described in [17]. The orbital-dependent one-electron potential is given by the derivative of Eq. (1) with respect to the orbital occupancy  $n_{m\sigma}$ :

$$V_{m\sigma}(\mathbf{r}) = V_{LDA}(\mathbf{r}) + \sum_{m'} (U_{mm'} - U_{eff}) n_{m'-\sigma} + \sum_{m' \neq m} (U_{mm'} - J_{mm'} - U_{eff}) n_{m\sigma} + U_{eff} \left( \frac{1}{2} - n_{m\sigma} \right) - \frac{1}{4} J \quad (2)$$

We define  $U_{eff} = U - J/2$ . The matrices  $U_{mm'}$  and  $J_{mm'}$  are calculated from the screened Slater integrals  $F^k$  ( $F^0, F^2, F^4$  for  $d$ -electrons), which are determined using the calculated values of  $U$  and  $J$  and the ratio of unscreened  $F^4/F^2$  [18].

Model calculations for the MX chain compounds usually use one-dimensional one- or two-band systems in which only the M  $d_{3z^2-r^2}$  and the X  $p_z$  orbitals are taken into account [12]. Experimentally, MX compounds have complicated structures of complex organic molecules ligands that are perpendicular to the chain axis and bonded to the M atoms. The bonding orbitals of the ligands are strongly hybridized with the  $d$  orbitals of the M atoms. The MX compounds are divided into three classes: (1) anionic, (2) cationic, and (3) neutral chains. The anionic chains have positive counterions so that the chains are negatively charged; in contrast, the cationic chains have negative counterions and are positively charged. The neutral chains have no counterions. We have studied a case of an anionic CDW chain  $K_4PtI_4PtI_6$ , and three cationic CDW and SDW chains  $[M(\text{chxn})_2][M(\text{chxn})_2X_2]X_4$  (chxn is 1,2-diaminocyclohexane,  $C_6H_{14}N_2$ ) with M= Ni (X= Br or Cl) or Pt with X= Cl.

*Cationic SDW chains*  $[Ni(\text{chxn})_2][Ni(\text{chxn})_2X_2]X_4$ . Depending on whether M is Pt or Ni, the associated MX chain shows a CDW or a SDW character, respectively [2-9,11-15]. For example, when MX is PtCl or PtBr, a Peierls instability is observed and the system is non-magnetic. When M is Ni and the counterion is Cl or Br, these systems are antiferromagnetic and exhibit no Peierls instability. [2,7,15]. We approximate the real structure by a simpler model structure in order to make a direct electronic-structure calculation feasible. The simplest model structure is to replace the  $(\text{chxn})_2$  by four ammonia units per each M atom (see Figure 1). For the model crystal structure we compress the lattice along the  $a$  axis so that the distance between ammonia on neighboring chains are similar to those for ammonia-ligand compounds [1]. We emphasize that in our model all coordinates of the atoms are the same as in real crystal structure except for the absence of the  $C_6H_{10}$  ring.

The local spin-density approximation (LSDA) alone can not reproduce the insulating magnetic ground-state of the SDW NiCl and NiBr systems. The electronic structure in the vicinity of Fermi level is very similar to that of the undoped cuprate superconductor materials, where LSDA calculations also predict a non-magnetic metallic state instead of the experimentally observed antiferromagnetic insulating state. This effect results from the LSDA magnetic transition being driven by the spin-polarization of a Stoner intraatomic

exchange interaction  $I$  (about 1 eV), instead of the much stronger Hubbard interaction  $U$  (about 8 eV).

Figure 2 shows the total density of states (DOS) and the energy dispersion along the chain direction  $\Gamma Z$  in the vicinity of Fermi level for the  $U = J = 0$  eV case. Despite the presence of the half-filled Ni  $d_{3z^2-r^2}$  band at the Fermi level the Peierls mechanism is not effective in opening the energy band gap. Instead, the small Ni-Ni distance sufficiently enhances the anharmonic elastic potential between Ni and Cl that the electron-phonon coupling (Peierls mechanism) is rendered ineffective. [9].

Figure 3 presents the Ni partial DOS at the vicinity of Fermi level decomposed into the various symmetries of the  $d$  channels for the calculated  $U$  and  $J$  as presented in Table 1 together with the dimerization, the magnetization and the energy band gap for all the systems studied here. The LDA+U calculated ground state remains undimerized and the the Hubbard term in Eq. (2) opens an energy band gap of 1.8 eV, in good agreement with the experimental value of 1.9 eV [15]. Further, a low-spin antiferromagnetic state with a magnetic moment of  $0.66 \mu_B$  is produced, which could be reduced by spin fluctuations neglected in the present study. The experimental value of the magnetic moment is not available at the present time. The low-spin antiferromagnetic state is due to the large octahedral ligand-field splitting  $\Delta_0 = e_g - t_{2g} \approx 4$  eV which produces a low-spin  $(t_{2g})^6(e_g)^1$  electronic configuration of the Ni<sup>+3</sup> ion. Figure 3 shows that, with respect to the the DOS projected on the Ni site, most of the weight of the  $(e_g)^1$  configuration comes from the  $d_{3z^2-r^2}$  orbital. Accordingly most of the contribution to the spin magnetic moment is from the polarized  $d_{3z^2-r^2}$  orbitals located in the vicinity of the band gap, and that only  $0.05 \mu_B$  is due to the polarization of the  $d_{x^2-y^2}$  orbitals. In addition, the optical band gap of 1.8 eV between the occupied Ni  $d_{3z^2-r^2}$  and the unoccupied Pt  $d_{x^2-y^2}$  is smaller than the antiferromagnetic gap of 2.3 eV arising from the splitting of the  $d_{3z^2-r^2}$  Pt bands. A slightly smaller value of  $U$  makes these two gaps comparable.

The properties of the NiBr system are very similar to that of NiCl: an antiferromagnetic insulator with a smaller gap of 1.28 eV [2,15]. Our calculation produces a Coulomb parameter

$U = 6.9$  eV, and an energy band gap of 1.6 eV with a spin magnetic moment value of  $0.63 \mu_B$ . Here also the contribution to the spin magnetic moment is mainly from the Ni  $d_{3z^2-r^2}$  orbitals.

*Cationic CDW chains*  $[\text{Pt}(\text{chxn})_2][\text{Pt}(\text{chxn})_2\text{Cl}_2]\text{Cl}_4$ . For PtCl the experimental value of the dimerization is 4.9% (the short Pt-Cl distance 2.32 Å and the long one 2.83 Å) [14].

The LDA + U calculation shows the absence of an antiferromagnetic SDW solution for this system (see Table 1) and a dimerization of 4%. The 0.8 eV band gap in the dimerized state is much smaller than the experimental gap of 1.6 eV. This disagreement in the band gap is not surprising, since LDA + U method works best for fairly localized orbitals with spin-orbital ordering like NiO [17]. For delocalized orbitals, without spin polarization, like the Pt  $5d$  LDA+U reduces essentially to the standard LDA. We should, in principle, use a model where the exchange correlation potential is non-local and dynamically screened, for example, the GW approximation of Hedin [19].

*Anionic CDW chain*  $\text{K}_4\text{PtI}_4\text{PtI}_6$ . This is a rather exotic material among the MX-chain family in that it does not have complicated organic ligands transversely bound to the metallic atom. We have chosen to study  $\text{K}_4\text{PtI}_4\text{PtI}_6$  (KPtI for short), because of the simplicity of the ligands (I). The structure could be described as  $\text{PtI}_6$  octahedra connected along the z-axis to form a chain, with K atoms located between the chains. While the measured structure is more complex [13] than the other systems computed in this Letter (including Pt-I-Pt angle smaller than  $180^\circ$  and disorder along the chain). We have modeled KPtI as a perfect linear chain without disorder.

The computed Hubbard parameter  $U$  (computed as described above) is 3.6 eV, and is much smaller than the typical 7 to 10 eV values for the antiferromagnetic late-transition-metal oxides [17]. This small value of  $U$  allows no antiferromagnetic SDW solution to the LDA +  $U$  equations for KPtI. At computed 3.9% dimerization, The 0.37 eV energy-gap is much smaller than the experimental value of 1.0 eV. Like the PtCl case, the underestimation of the band gap is due to the inadequacy of LDA + U in handling delocalized electrons.

Several differences between PtCl and KPtI arise from the fact that Pt-N distance (2.06

Å) is much shorter than the Pt-I distance (2.65 Å), and Pt-Pt distance in PtCl (5.16 Å) is much shorter than the 5.91 Å in KPtI. In comparing PtCl to KPtI we found that PtCl has (i) a much stronger 5*d*-ligand hybridisation, (ii) a larger Pt  $d_{x^2-y^2}$ - $d_{3z^2-r^2}$  energy separation, and (iii) a larger CDW reflected by the larger  $Pt^{3-\delta} \rightarrow Pt^{3+\delta}$  charge transfer (0.29 electron in PtCl versus 0.14 electron in KPtI).

We have studied examples of both anionic and cationic linear MX-chain compounds by means of a parameter-free, mean-field, multi-orbital Hubbard model implemented around the LDA. For the cationic NiX (X= Br or Cl) chains, where the 3*d* orbitals are much more localized than the 5*d* of Pt, the predicted energy band gap is found to be very close to the experimental one. The model also predicts that the NiX chains have an undimerized antiferromagnetic ground-state in agreement with experiment. On the other hand, in PtCl and KPtI the band gap was found to be much smaller than the measured optical gaps.

We thank A. R. Bishop, T. J. Gammel, B. I. Swanson, G. Kanner, B. Scott, and A. Saxena for their interest in this work. We acknowledge partial support provided by the Department of Energy (DOE) - Basic Energy Sciences, Division of Materials Sciences. Supercomputer time was provided by the Ohio Supercomputer and by the DOE.

## REFERENCES

- [1] H. J. Keller, in *Extended Linear Chain Compounds*, Vol. 1, ed. by J. S. Miller (Plenum Press, NY, 1983), p. 357; R. J. H. Clark and R. E. Hester, in *Infrared and Raman Spectroscopy*, ed. by R. J. H. Clark and R. E. Hester (Heyden, 1984), Vol. 11, p. 95.
- [2] H. Okamoto *et al.*, Phys. Rev. B **42**, 10381 (1990), and references therein.
- [3] H. Okamoto *et al.*, Synth. Metals, 41-43, 2791 (1991).
- [4] H. Okamoto *et al.*, Mat. Sc. and Eng., **B13**, L9 (1992).
- [5] R. J. Donohoe *et al.*, in *Frontiers of High Pressure Research*, ed. by H. D. Hochheimer (Plenum Press, NY, 1991).
- [6] B. Scott *et al.*, Synthetic Metals, **55-57**, 3426 (1993).
- [7] M. Yamashita *et al.*, Synth. Metals, **55-57**, 3461 (1993).
- [8] M. Alouani *et al.*, Phys. Rev. Lett. **69**, 3104 (1992).
- [9] M. Alouani *et al.*, Phys. Rev. Lett. **71**, 1415 (1993).
- [10] X. Z. Huang and A. R. Bishop, Phys. Rev. B. **48**, 16148 (1993).
- [11] D. Baeriswyl and A. R. Bishop, J. Phys. C **21**, 339 (1988).
- [12] J. T. Gammel *et al.*, Phys. Rev. B **45**, 6408 (1992).
- [13] G. Thiele *et al.*, Naturwiss. **65**, 206 (1978).
- [14] K. P. Larsen and H. T. Toftlund, Acta Chemica Scand. **A31**, 182 (1977).
- [15] K. Toriumi *et al.*, Mol. Cryst. Liq. Cryst. **181**, 333 (1990).
- [16] V. I. Anisimov *et al.*, Phys. Rev. B **48**, 16929 (1993).
- [17] V. I. Anisimov and O. Gunnarsson, Phys. Rev. B **43**, 7570 (1991).
- [18] F.M.F. de Groot *et al.*, Phys. Rev. B **42**, 5459 (1990).



[19] L. Hedin, Phys. Rev. **139**, A796 (1965).

## FIGURES

FIG. 1. Schematic structure of a single cationic  $M(\text{chxn})_2[\text{Ni}(\text{chxn})_2\text{X}_2]\text{X}_4$ . The chxn ( $\text{N}_2\text{C}_6\text{H}_{14}$  ligand structure is represented in more detail in the insert (a), and the simplified structure used in the model calculation is represented in the insert (b), where the cyclohexane is replaced by two H atoms.

FIG. 2. LDA total DOS and energy dispersion along the chain direction  $\Gamma Z$  in the vicinity of Fermi level (5  $\mathbf{k}$ -points are used along the  $\Gamma Z$  direction). Although only one band of Ni  $d_{3z^2-r^2}$  character crosses the Fermi level, the Peierls instability is not effective in opening an energy band gap. This is because the elastic anharmonic potential between Ni and Cl ions along the chain is stronger than the electron-phonon coupling.

FIG. 3. LDA+U DOS in the Ni site at the experimental lattice parameter decomposed into various  $d$ -channel symmetries: (a) for majority spin, and (b) for minority spin (The spin-up of a Ni atom is the down-spin of its nearest-neighbor Ni atoms and visa-versa). The dark shaded area represent the Pt  $d_{3z^2-r^2}$  weight, and the light shaded area the  $d_{x^2-y^2}$  weight (the occupation numbers of the  $d_{3z^2-r^2}$  and  $d_{x^2-y^2}$  orbitals are  $n_{d_{3z^2-r^2}}^\uparrow = 1.0$ ,  $n_{d_{3z^2-r^2}}^\downarrow = 0.39$ ,  $n_{d_{x^2-y^2}}^\uparrow = 0.65$ , and  $n_{d_{x^2-y^2}}^\downarrow = 0.60$ ). The Hubbard term in Eq. (2) opens the energy band gap at the Fermi level of 1.8 eV and produces an antiferromagnetic ground state. Almost the entire contribution to the spin magnetic moment of  $0.66 \mu_B$  is from  $d_{3z^2-r^2}$  orbitals, whereas only  $0.05 \mu_B$  is due to the polarization of the  $d_{x^2-y^2}$  orbitals.

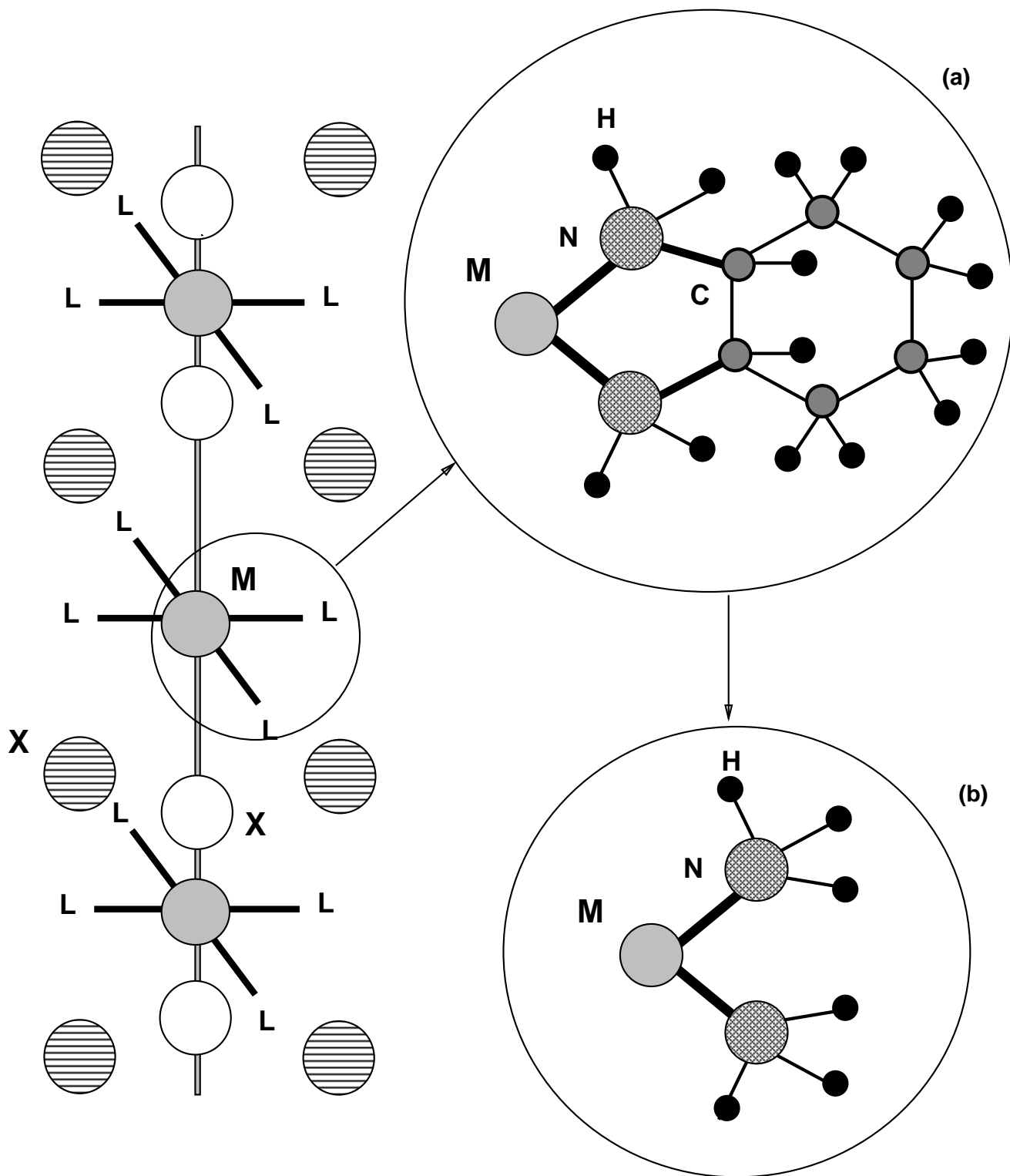
## TABLES

TABLE I. Calculated dimerization, magnetic moment, and band gap for KPtI, PtCl, NiBr, and NiCl compared to the available experimental results indicated in parentheses.

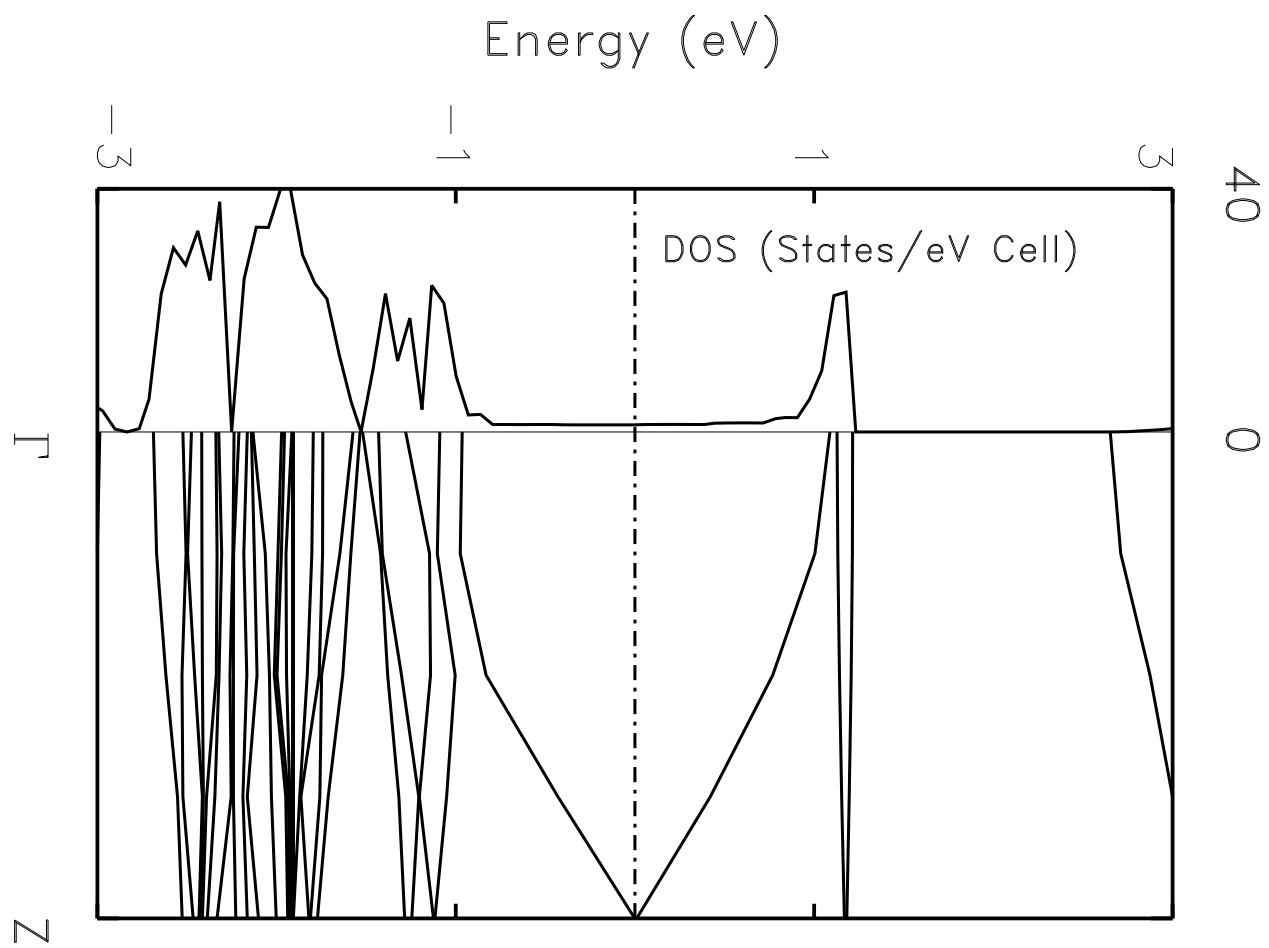
|      | M-M (Å)              | U (eV) | J (eV) | Dimerization (%)        | Magnetic moment ( $\mu_B$ ) | Band gap (eV)            |
|------|----------------------|--------|--------|-------------------------|-----------------------------|--------------------------|
| PtI  | (5.91 <sup>a</sup> ) | 3.6    | 1.0    | 3.9 (4.1 <sup>a</sup> ) | 0                           | 0.4 (1.0 <sup>a</sup> )  |
| PtCl | (5.16 <sup>b</sup> ) | 3.5    | 1.0    | 4.0 (4.9 <sup>d</sup> ) | 0                           | 0.8 (1.6 <sup>c</sup> )  |
| NiBr | (5.16 <sup>e</sup> ) | 6.9    | 0.7    | 0 (0 <sup>d</sup> )     | 0.63                        | 1.6 (1.28 <sup>e</sup> ) |
| NiCl | (4.89 <sup>e</sup> ) | 6.8    | 0.7    | 0 (0 <sup>e</sup> )     | 0.66                        | 1.8 (1.9 <sup>e</sup> )  |

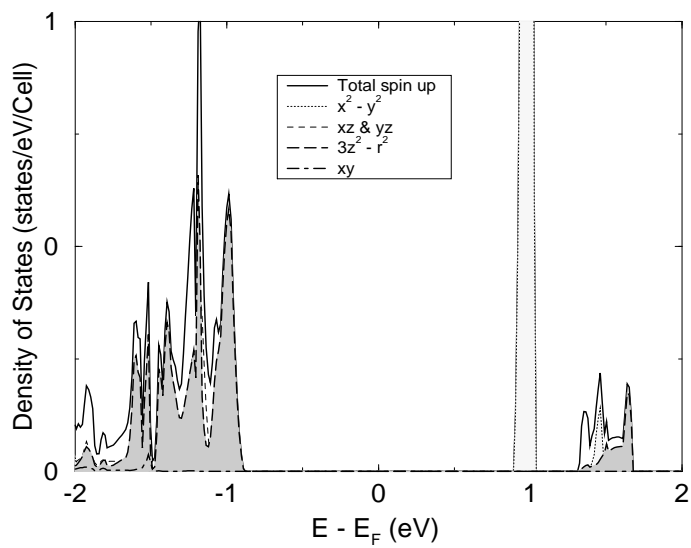
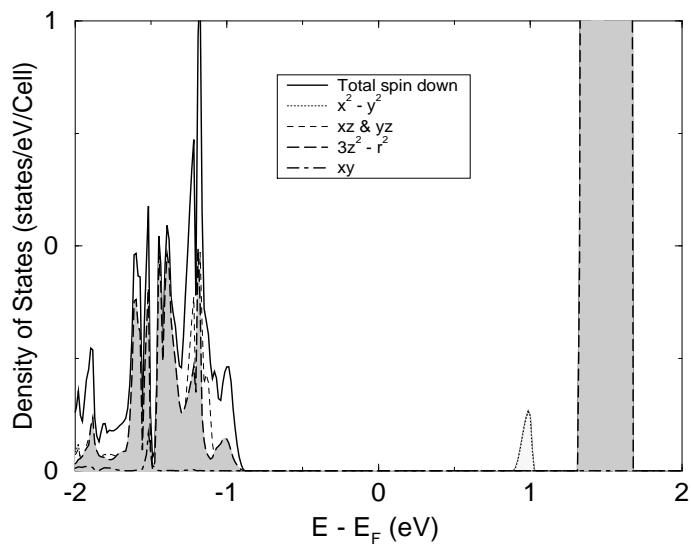
<sup>a</sup>

<sup>a</sup> Ref. [13]   <sup>b</sup> Ref. [14]   <sup>c</sup> Ref. [6]   <sup>d</sup> Ref. [2]   <sup>e</sup> Ref. [15]



V. I. Anisimov et al. Fig. 1





V. I. Anisimov *et al.*  
 Fig. 3